# A Non-Charge-Sheet Based Analytical Model of Undoped Symmetric Double-Gate MOSFETs Using SPP Approach

Jin He, Xuemei Xi, Mansun Chan*, Chung-Hsun Lin, Ali Niknejad, and Chenming Hu
Department of EECS, University of California at Berkeley, CA, 94720
*Department of EEE, HKUST, Clear Water Bay, Kowloon, Hong Kong
E-mail: jinhe@eecs.berkeley.edu

## Abstract

*A non-charge-sheet based analytical model of undoped symmetric double-gate MOSFETs is developed in this paper using the SPP approach. The essential difference of the present theory compared with the previous lies in that the Poisson equation is solved in the term of the electron concentration rather than the term of the surface potential. This solution formulates electrical field, surface potential in inversion charge term rather than the surface potential. Thus, a non-charge-sheet-based analytical solution of inversion charge is obtained directly replacing solution of transcendent equation groups of the surface potential. The obtained inversion charge relation then serves to develop a non-charge-sheet-based analytical theory for undoped symmetric double-gate MOSFETs from Pao-Sah current formulation. . The formulated model has an analytic form that does not need to solve for the transcendent equation as in the conventional surface potentials or Pao-Sah formulation. The validity of the model has also been demonstrated by extensive comparison with AMD double-gate MOSFET's data*

## 1. Introduction

As CMOS technologies are scaling down beyond 50nm node, the undoped (or lightly-doped) double-gate MOSFETs are becoming the most promise candidate device structure because of the advocated advantages such as ideal 60 mV/decade subthreshold slope, volume inversion, free-dopant-associated fluctuation effects and mobility degradation, etc[1-3]. Compact modeling of this structure has been extensively studied. Most of these were based on surface potential based charge-sheet approximation[4-7]. Since there exists volume inversion in double-gate MOSFETs, however, the physics picture of carrier distribution within a zero-thickness sheet is more or less accurate for modeling of double-gate MOSFET's characteristics. For an ultra-thin double gate MOSFET, the charge-sheet approximation cannot be used because the inversion layer thickness is comparable with silicon film thickness and the model loses its accuracy. In a recent work, a one-dimensional (1-D) Poisson-Boltzamnn equation was solved for the double-gate MOSFET to derive analytical solution for surface potential and inversion charge density[8-9]. This result serves as a core foundation for developing non-charge-sheet-based model[10]. Due to the numerical complexity and time consuming nature of iteration technique, this surface-potential based non-charge-sheet model is still tedious for practical compact application.

In fact, the analytical solution of surface potential in bulk MOSFETs is already difficult enough. In double gate MOSFETs, the presence of gate couple effect and center potential dependence on the surface potential further prevent obtaining an exact analytical solution of the surface potential in terms of the biases. However, the analytical solution is highly desirable since precise description of at least up to the third order derivative with respect to the bias voltages is generally required for performing correct distortion analysis among other reasons. The requirement and the difficulty in calculating surface potential and saturation point make us re-think how to develop basis of double-gate MOSFEs. BSIM3/4 model directly calculate the inversion charge in terms of bias[11]. USIM, UUCM, EKV and ACM have also contributed efforts in modeling inversion charge[12-15]. These works indicate that a charge-based MOSFET model is direct, and computationally efficient in modeling I-V and C-V characteristics.

Using our developed Surface-Potential-Plus (SPP) approach[16-18], a non-charge-sheet-based analytical model of undoped symmetric double-gate MOSFETs is developed in this paper by solving carrier concentration equation and combining the Pao-Sah current formulation. The essential difference of the SPP approach compared with the previous lies in that the Poisson equation is solved in the term of the electron concentration rather than the term of surface potential. This solution formulates electrical field, surface potential in inversion charge term rather than the surface potential. Thus, a non-charge-sheet-based analytical solution of inversion charge is obtained replacing solution of transcendent equation groups of the surface potential. The solution gives exact analytical expressions of channel mobile charge, electrical field and potential as an explicit function of silicon thickness and biases. The obtained inversion charge relation is used to develop a non-charge-sheet-based model of undoped double-gate MOSFET from Pao-Sah current formulation. One should note that the obtained inversion charge and current are quite same with that of SPP bulk model, representing re-thinking and new direction in MOSFET compact modeling development. The analytical model has also been verified by AMD double-gate MOSFET's data.

## 2. Analytical theory

Fig. 1 shows the coordinate and energy level

0-7695-2093-6/04 $20.00 © 2004 IEEE

distribution diagrams of a symmetric double-gate MOSFET. Same voltage is applied to the two gates having the same work function. Since there is no contact to the silicon body, the energy levels are referenced to the electron quasi-Fermi level of the source and drain. Here we consider an nMOSFET with the potential is larger than the thermal voltage so that the hole is negligible. However, the equation and derivation easily extend to pMOSFETs only through changing sign of the potential, field and polarization of carriers.

One can write Poisson's equation for the silicon region with only the mobile charge (electron) density as

$$\frac{d^2\phi}{dx^2} = \frac{qn}{\varepsilon_{si}} \tag{1}$$

where n is the electronic charge, $\varepsilon_{si}$ is the permittivity of silicon. According to Boltzmann statistics, the mobile electron concentration is expressed by the potential

$$n = n_i \exp\left(\frac{q(\phi - V_{ch})}{kT}\right) \qquad n_0 = n_i \exp\left(\frac{q(\phi_0 - V_{ch})}{kT}\right) \tag{2}$$

The spatial derivative of the electron concentration is

$$\frac{d\phi}{dx} = \frac{kT}{qn}\frac{dn}{dx} \tag{3}$$

$$\frac{d^2\phi}{dx^2} = \frac{kT}{qn}\frac{d^2n}{dx^2} - \frac{kT}{qn^2}\left(\frac{dn}{dx}\right)^2 \tag{4}$$

substitution (4) into (1) gives a final equation for electron concentration

$$\frac{d^2n}{dx^2} = \frac{1}{n}\left(\frac{dn}{dx}\right)^2 + \frac{q^2n^2}{\varepsilon_{si}kT} \tag{5}$$

This normal differential equation has two mathematical solutions, one is trigonometric function and another is the hyperbolic function.

$$n(x) = \frac{c_0}{\cos^2\left[\left(\frac{q^2c_0}{2\varepsilon_{si}kT}\right)^{1/2} x\right]} \tag{6a}$$

$$n(x) = \frac{c_0}{\cosh^2\left[\left(\frac{q^2c_0}{2\varepsilon_{si}kT}\right)^{1/2} x\right]} \tag{6b}$$

The choice of the electron distribution function depends on the reference coordinate. If the coordinate reference zero point is the silicon film center, the trigonometric function has to be chosen. If the coordinate reference zero point is the silicon film surface, the hyperbolic function has to be chosen.

For consistent with the common treatment and mathematical simplicity of a model, a physics reasonable analytical solution for our case is to choose the former. In this case, $x = 0$, $n(x) = n_o$, (6) is further simplified into

$$n(x) = \frac{n_0}{\cos^2\left[\left(\frac{q^2n_0}{2\varepsilon_{si}kT}\right)^{1/2} x\right]} \tag{7}$$

Substitution of (7) into (1) gives the corresponding electrical field and potential distributions in the silicon film

$$\phi(x) - \phi_0 = \frac{kT}{q}\ln\cos^{-2}\left[\left(\frac{q^2n_0}{2\varepsilon_{si}kT}\right)^{1/2} x\right] \tag{8}$$

$$E(x) - E(x_0) = \left[\frac{2n_0kT}{\varepsilon_{si}}\right]^{1/2} \tan\left[\left(\frac{q^2n_0}{2\varepsilon_{si}kT}\right)^{1/2} x\right] \tag{9}$$

The symmetry of boundary condition of double gate makes the electric field of the center of the silicon film is zero. If this center is chosen as the reference coordinate zero point, then, the surface potential and the surface electric field are given simply, respectively

$$\phi_s = \frac{kT}{q}\ln\left[\frac{n_0}{n_i}\cos^{-2}\left[\left(\frac{q^2n_0}{2\varepsilon_{si}kT}\right)^{1/2}\frac{T_{si}}{2}\right]\right] \tag{10}$$

$$E_s = \left[\frac{2n_0kT}{\varepsilon_{si}}\right]^{1/2} \tan\left[\left(\frac{q^2n_0}{2\varepsilon_{si}kT}\right)^{1/2}\frac{T_{si}}{2}\right] \tag{11}$$

If we define $Q_{in} = q\int_0^{T_{si}/2} n(x)dx$, then, the half of total inversion charge can be expressed

$$Q_{in} = \left[2\varepsilon_{si}n_0kT\right]^{1/2} \tan\left[\left(\frac{q^2n_0}{2\varepsilon_{si}kT}\right)^{1/2}\frac{T_{si}}{2}\right] \tag{12}$$

In practice, the surface potential, field and carrier concentration are controlled by applying a gate voltage. According to Gauss's law, the total applied gate voltage is

$$V_G - \Delta\psi_i = \phi_S + E_{ox}t_{ox} = \phi_s + \frac{Q_{in}}{\varepsilon_{ox}}t_{ox} \tag{13}$$

where $\Delta\psi_i$ is the work function difference.

Substituting the surface potential and inversion charge expressions into (13) results in

$$V_G - \Delta\psi_i - V_{ch} = \frac{kT}{q}\ln\left[\frac{n_0}{n_i}\cos^{-2}\left[\left(\frac{q^2n_0}{2\varepsilon_{si}kT}\right)^{1/2}\frac{T_{si}}{2}\right]\right] + \frac{\varepsilon_{si}}{\varepsilon_{ox}}t_{ox}\left[2n_0\varepsilon_{si}kT\right]^{1/2}\tan\left[\left(\frac{q^2n_0}{2\varepsilon_{si}kT}\right)^{1/2}\frac{T_{si}}{2}\right] \tag{14}$$

Eq.(14) gives the exact closed form expression of electron concentration at the silicon film center as a function of gate voltage, channel voltage, and silicon film. The electron concentration, field and potential distribution and its surface values can be obtained precisely for calculated $n_0$. This form is useful because of its precise and solid physics biases, it is, however, too complex due to transcendent equation characteristics.

The following analysis shows that formulating the electrical field and surface potential in the term of inversion charge will greatly simplify the related equations. The inversion charge expression repeats here

$$Q_{in}^2 = 2\varepsilon_{si} n_0 kT \tan^2\left[\left(\frac{q^2 n_0}{2\varepsilon_{si} kT}\right)^{1/2}\frac{T_{si}}{2}\right] = 2\varepsilon_{si} n_0 kT \frac{\sin^2\left[\left(\frac{q^2 n_0}{2\varepsilon_{si} kT}\right)^{1/2}\frac{T_{si}}{2}\right]}{\cos^2\left[\left(\frac{q^2 n_0}{2\varepsilon_{si} kT}\right)^{1/2}\frac{T_{si}}{2}\right]} \quad (15)$$

We will use the inversion charge expression to replace the surface potential term in Eq.(13). This surface potential term comes into effect only in the sub-threshold region. In this region, the potential distribution is almost flat and the volume inversion occurs [2, 5]. In this sub-threshold region case, the entire channel region contributes to conduction, and the inversion charge is almost proportional to the silicon film thickness, thus it can be given[2,5]

$$Q_{in} = qn_0 T_{si}/2 \quad (16)$$

On the other hand, since the tan function of the inversion charge expression is mainly determined by cosine function, an exact approximation is used for sine function so to simplify this function expression combining (16).

$$\sin^2\left[\left(\frac{q^2 n_0}{2\varepsilon_{si} kT}\right)^{1/2}\frac{T_{si}}{2}\right] \approx \left(\frac{q^2 n_0}{2\varepsilon_{si} kT}\right)\frac{T_{si}^2}{4} \approx \frac{qQ_{in}}{2\varepsilon_{si} kT}\frac{T_{si}}{2}\exp(f) \quad (17a)$$

This approximation works well for ultra-thin silicon case, leading to a negligible error. In fact, this error compared to Poisson-Boltzmann equation solving to derive surface potential and inversion charge density is less 2% in all operation region. In order to compensate the error leaded by this approximation, we use a dimensionless correction factor $f$. This factor should be a step function of the gate voltage, e.g. equal to unit below the threshold point and zero above the threshold point. An exact approximate solution of this factor is written as

$$f = \left[\frac{\tanh(v_G - \Delta\phi_i)}{v_G - \Delta\phi_i}\right]^2 \quad (17b)$$

via comparison with the numerical result. In this case, this total error is less 0.5%. Then, we have

$$\sin^2\left[\left(\frac{q^2 n_0}{2\varepsilon_{si} kT}\right)^{1/2}\frac{T_{si}}{2}\right] = \frac{qQ_{in}}{2\varepsilon_{si} kT}\frac{T_{si}}{2}\exp(f) \quad (17c)$$

Making use of this approximation, (16) is written as

$$Q_{in} = \frac{qn_0 T_{si}/2}{\cos^2\left[\left(\frac{q^2 n_0}{2\varepsilon_{si} kT}\right)^{1/2}\frac{T_{si}}{2}\right]} \quad (18)$$

Substitution of (18) into (13) and replacing the surface potential gives

$$V_G - \Delta\psi_i - V_{ch} + \frac{fkT}{q}\ln(qn_i T_{si}/2) = \frac{kT}{q}\ln Q_{in} + \frac{Q_{in}}{\varepsilon_{ox}/t_{ox}} \quad (19)$$

This inversion charge equation is quite same with that of SPP model, except the sub-threshold slope n is replaced with 60mV. Thus, it is very easy to obtain the IV and CV characteristics following SPP model.

The all biases are normalized by $kT/q$ and inversion charge is normalized by $C_{ox}kT/q$, (19) is simplified into

$$v_G - \Delta\phi_i - v_{ch} + f\ln\left(\frac{q^2 n_i T_{si} t_{ox}}{2kT\varepsilon_{ox}}\right) = \ln q_{in} + q_{in} \quad (20)$$

The inversion charge in (20) can be solved explicitly in terms of the Lambert W function to yield the following exact expression

$$q_{in} = W_0\left[\exp\left(v_G - \Delta\phi - v_{ch} + f\ln\left[\frac{q^2 n_i T_{si} t_{ox}}{2kT\varepsilon_{ox}}\right]\right)\right] \quad (21a)$$

where $W_0$ stands for the usual short-hand notation used for the principal branch of the ''Lambert-W'' function.

The exact solution that we propose makes use of the principal branch of the Lambert W function which is defined as the solution to the equation $We^W = x$. The Lambert *W* function is a popular function in numerous physics applications [18]. It has also been used to provide solutions to previously unsolved basic diode and bipolar transistor circuit analysis. This function has also been incorporated into some circuit simulation tools and software packages such as Mathematica and Maple, and readily for use.

Once the inversion charge is obtained, to model CV characteristics of undoped double gate MOSFET is easy. The following discussion focuses on how to model IV characteristics. According to Pao-Sah model, the current including the diffusion and drift component is written as

$$I_{ds} = \mu w C_{ox}\left(\frac{kT}{q}\right)^2 q_{in}\frac{dv_{ch}}{dy} \quad (22)$$

For constant gate voltage, the differentiation of (20) is written as

$$dv_{ch} = dq_{in}/q_{in} + dq_{in} \quad (23)$$

Substitution of (23) into (22) gives

$$I_{ds} = \mu w C_{ox}\left(\frac{kT}{q}\right)^2 (q_{in}dq_{in} + dq_{in}) \quad (24)$$

As a result, we get the analytical current expression

$$I_{ds} = \frac{\mu w}{L}C_{ox}\left(\frac{kT}{q}\right)^2\left[\frac{q_s^2 - q_d^2}{2} + (q_s - q_d)\right] \quad (25)$$

Considering double gate control characteristics. The final current should double.

One should note that the final current expression is quite same with that of SPP model. Thus, this result has great convenient and simplification for IV and CV modeling. First, using SPP approach, small dimensional effects of undoped double gate MOSFET can be included in this unfied current expression; Second, this current form direct gives the inversion charge, surface potential distribution along the channel direction also greatly simplifies the trans-capacitance and trans-conductor modeling compared with that of the surface-potential-based model. Finally, more important, this current form also directly gives the exact analytical expression of the saturation inversion charge, saturation surface potential thus saturation drain voltage. This is almost impossible for the surface-potential-based model.

## 3. Result and discussion

### 3.1 Electron and potential distribution in the silicon film

Fig.2 demonstrate the electron concentration and electrical potential distribution in the silicon film predicted by the analytical model for three different effective gate voltages. Compared to the slight change of the potential distribution, the electron concentration shows significant exponential relationship with increase of the gate voltage. However, the electron distribution is almost flat in the sub-threshold region. In this sub-threshold region case, $Q_{in} = qn_0T_{si}/2$ is a good approximation to the inversion charge density, as shown in Eq.(17a). With increase of the effective gate voltage, the device goes into the strong inversion region where the surface electron concentration shows several order higher than that of the silicon film center. In this case, device behaves like a surface channel bulk MOSFET and the surface electron concentration dominates the inversion charge density, Eq.(17) is invalid here. However, the effect of this term of Eq.(17) is almost negligible and the linear term dominates in Eq.(20) in this strong inversion case.

### 3.2 Surface potential and inversion charge dependence on the bias

Fig.3 presents the carrier charge per unit area in the channel versus the applied gate voltage, as calculated with (20), for three values of channel voltage. There are two distinct regions of operation in the undoped bulk MOSFET, just like in a conventional bulk with gate voltage is clearly seen in Fig.3(b) at values well above the threshold voltage. One significant result is the relation between the inversion charge density and the channel voltage. Contrast to the gate voltage, Fig.2 indicates that the channel voltage makes the inversion charge decrease exponentially in the sub-threshold region and linearly in the strong inversion region. This result coincides well with (20). Below the threshold voltage, the mobile charge density is low and increases exponentially with the gate voltage with the sub-threshold slope of 60mV, as shown Fig.3(a). However, the expected linear increase of the carrier charge-sheet density

Fig.4 presents the surface potential versus gate voltage characteristics obtained using (13) for an undoped DG MOSFETs. Evidently, there also have two distinct regions of operation in the undoped DG MOSFET, just like in a conventional bulk MOSFET. Below the threshold, the surface potential almost increases linearly with the gate voltage. In the region, the effect of the inversion charge is almost negligible. However, once above the threshold, the surface potential has to increase logarithmically with the gate voltage, shows the contribution of the inversion charge. As in the conventional bulk MOSFETs, the channel voltage makes the surface potential almost increase linearly in the strong inversion region but almost negligible in the sub threshold region as shown in Fig.3 (a). On interesting result is that the oxide layer has a slight effect on the surface potential in strong inversion region and almost no effect on the sub-threshold region in the undoped DG MOSFETs. This physics picture is in contrast with the conventional bulk MOSFEs where the sub-threshold region slope has a strong dependence on the oxide thickness.

### 3.3 Volume inversion

Fig.5 demonstrate the effect of the silicon film thickness on the inversion charge versus gate characteristics. It is very interesting that the silicon film thickness makes the sub-threshold inversion charge increases while almost no effect on the strong inversion charge density. This is the volume inversion case that decrease of the silicon thickness can effectively control the sub-threshold region leakage current. Thus, the volume inversion increases the sub-threshold region leakage. In the device practice, we cannot expect the volume inversion to occur because of standby power consideration.

### 3.4 I-V characteristics

In order to verify the analytical model, we use this model to simulate a well-temped undoped double-gate MOSFET with the channel length of 10um and gate oxide thickness of 30A and silicon thickness of 20nm. Fig.6 and Fig.7 show the undoped MOSFET current voltage characteristics predicted by the presented analytical model with the constant mobility of $400\,cm^2/V.s$. The continuity of this model keeps well from the sub-threshold region to the strong inversion region for the different drain bias conditions, as shown in Fig.6. One important result is that the drain voltage has no effect on the sub-threshold current but increases the strong inversion current. The result of Fig.7 indicates that the double gate MOSFET shows good saturation characteristics, verifying the validity of the analytical model. Fig.8 shows a preliminary comparison of Ids-Vg and Ids-Vds characteristics between the analytical model and the AMD data for 106nm DG MOSFET. Fig.9 demonstrate the comparison between the analytical model and the experimental result from AMD double-gate MOSFET's data. The analytical model uses SPP modules on SCE, DIBL, QME, and unified mobility model in DG model. A good agreement is found between both.

## 4. Conclusion

Design and modeling of undoped symmetric double-gate MOSFETs would benefit from computationally efficient and physically meaningful compact models. In this paper, we have developed a non-charge-sheet based analytical model for this structure based on the device

physics. The exact analytical solution of the electron concentration and density as an explicit function of the gate voltage and silicon film, valid for all device operation region is derived and this solution with Pao-Sah current formulation gives the analytical current expression. The validity of the analytical model is also verified by the experimental data.

**Acknowledgement:** This work was supported by SRC under the contract number 2002-NJ-1001 and partially supported by a grant from RGC of Hong Kong under the number HKUST6111/03E. We also thank AMD Corporation for providing experimental data and Prof. Taur from UC of San Diego for useful discussion.

## References

[1] D. Frank, S. Laux, and M. Fischetti, "Monte Carlo simulation of a 30-nm dual-gate MOSFET: How far can silicon go?," in *IEDM Tech. Dig.*, p. 553, 1992.
[2] F. Balestra, S. Cristoloveanu, M. Benachir, J. Brini, and T. Elewa, "Double-gate silicon-on-insulator transistor with volume inversion: A new device with greatly enhanced performance," *IEEE Electron Device Lett.*, vol. EDL-8, p. 410, 1987.
[3] T. Tanaka, K. Suzuki, H. Horie, and T. Sugii, "Ultrafast low-power operation of p -n double-gate SOI MOSFETs," in *Proc. VLSI Technol. Symp. Tech. Dig.*, p. 11, 1994,.
[4] C.Mallilarjun and K.N.Bhat, "Numerical and charge-sheet models for thin-film SOI MOSFETs". IEEE Trans Electron. Devices, 37(9), pp.2039-2051, 1990.
[5] K.Suzuki, T.Tanaka, Y.Toshiharu, H.Horie, Y.Arimoto and T.Itoh, " Analytical surface potential expression for thin-film double-gate SOI MOSFETs". Solid State Electronics. vol.37(2), pp.327-332, 1994.
[6] Email Arnold, "Double-charge-sheet model for thin silicon-on-inslulation films" *IEEE Trans. Electron Devices*, vol. 49, pp. 2143–2153, Dec. 1996.
[7] T.Nakagawa, T.Sekigawa, T.Tsutsumi, E.Suzuki and H.Koike, " Primary consideration on compact modeling of DG MOSFETs with four-terminal operation mode". Nanotech 2003, vol.2, MSM, pp.330-333, 2003.
[8] Y. Taur, "Analytic solutions of charge and capacitance in symmetric and asymmetric double-gate MOSFETs," *IEEE Trans. Electron Devices*, vol. 48, pp. 2861–2869, Dec. 2001.
[9] Y. Taur, "An analytical solution to a double-gate MOSFET with undoped body," *IEEE* Electron Device Lett., vol. 21, pp. 245–247, July, 2000.
[10] Y. Taur, Xiaoping Liang, and Wei Wang, "non-charge-sheet based continuous I-V model for double-gate MOSFETs", submitted to 2003' IEDM.
[11]BSIM, http://www.device.eecs.berkeley.edu/~bsim3.
[12]C.Enz, F.Krummenacher, and E.Vittoz. " An analytical MOS transistor model valid in all regions of operation and dedicated to low-voltage and low-current application". Analog integrated circuits and signal processing. vol.8, 83-114, 1995.
[13]H. Gummel and K.Singhal. "Inversion charge modeling". IEEE Trans on Electron Devices, vol. 48, 1585-1593, 2001.
[14] C.K.Park,C.Y.Lee,B.J.Moon and Y.H.Byun et al., " A unified current-voltage model for long channel nMOSFET's" . IEEE Trans Electron Devices, vol.38, 399-406, 1991.
[15] O.C.Gouveia-F,A.I.A.Cunha,.http://www.dolphin.fr.
[16] Jin He, Xuemei Xi, Mansun Chan, Ali Niknejad, and Chenming Hu, "Surface-Potential-Plus: An Advanced MOSFET Model". Nanotech 2003, vol.2, MSM, pp.262-265, 2003.
[17] Mansun Chan, Y.Taur, C.H.Lin, Jin He, Mansun Chan, Ali Niknejad, and Chenming Hu, " A framework for generic physics based double-gate MOSFET modeling". Nanotech 2003, vol.2, MSM, pp.270-273, 2003.
[18] Jin He, Xuemei Xi, Mansun Chan, Ali Niknejad, and Chenming Hu, "An exact analytical model of undoped body MOSFETs using the SPP approach". MSM'2004.

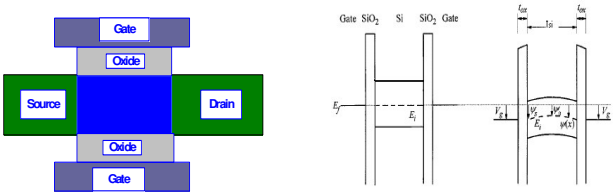


Fig.1. Diagrams of the structure and energy levels of undoped double-gate MOSFETs.

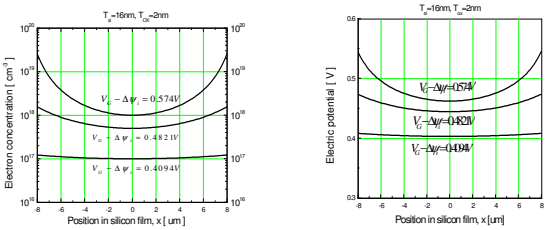


Fig.2. The mobile electron and potential distribution as a function of the silicon film thickness for DG MOSFETs .

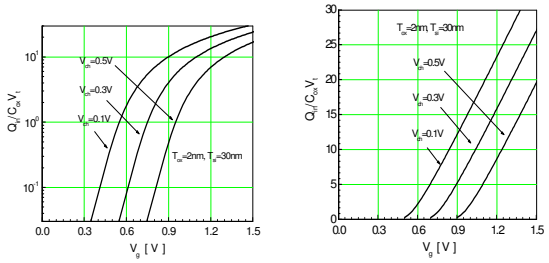


Fig.3. The mobile carrier density as a function of channel voltage with the different silicon thickness and gate voltage for undoped MOSFETs with symmetric double-gate structure.

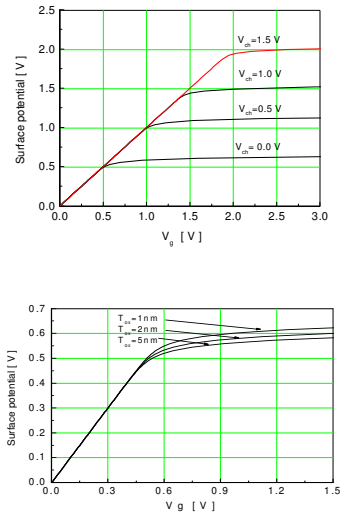


Fig.4 Surface potential versus gate voltage with the different channel voltage and oxide thickness.

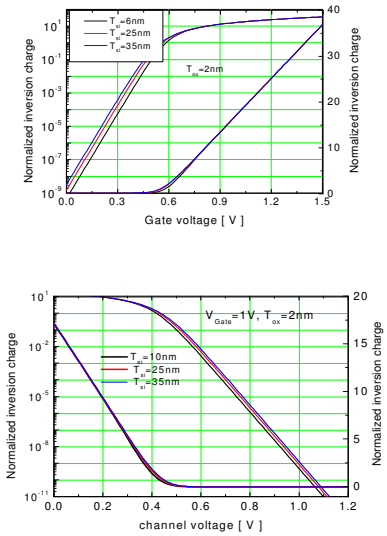


Fig.5 The mobile carrier density as a function of gate voltage and channel voltage with the different silicon thickness for undoped DG MOSFETs.

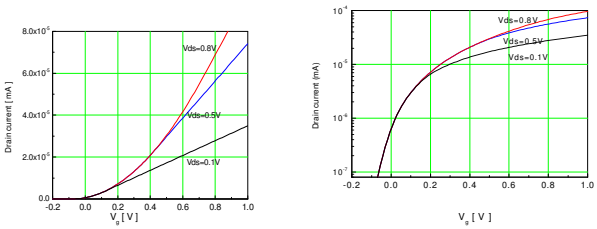


. Fig.6. The drain current versus the gate voltage with the different drain voltage for a 10um undoped MOSFETs with symmetric double-gate structure.

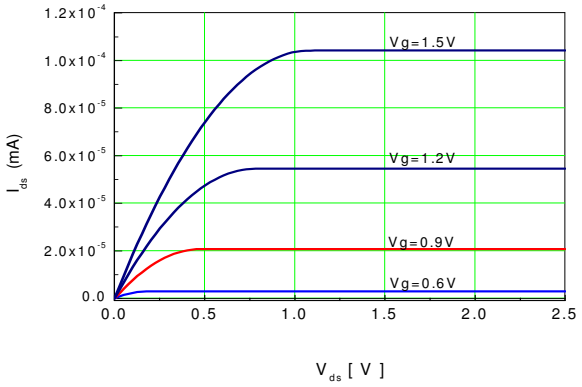


Fig.7. The drain current versus the drain voltage with the different gate voltage for a 10um undoped DG MOSFET.

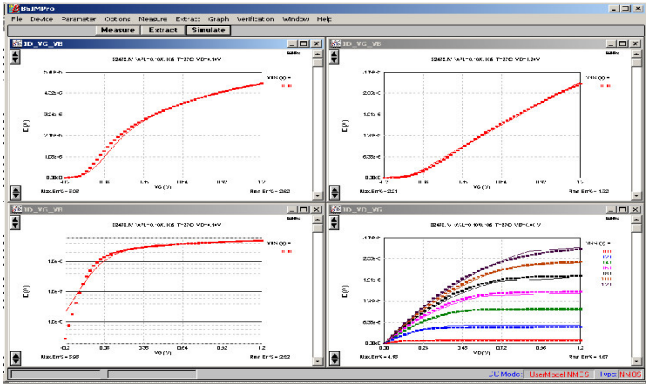

Fig.8 Comparison of Ids-Vg and Ids-Vd characteristics between the analytical model and AMD data for 106nm channel of DG MOSFET.

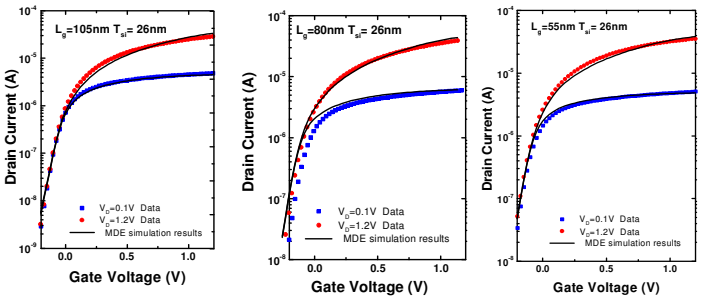


Fig.9 Comparison between the analytical model and AMD double-gate data.